Geosci. Model Dev. Discuss., doi:10.5194/gmd-2017-68, 2017
Manuscript under review for journal Geosci. Model Dev.
Discussion started: 25 April 2017
© Author(s) 2017. CC-BY 3.0 License.

Geoscientific Model Development Discussions

The "ABC model" (Vn 1.0): a non-hydrostatic toy model for use in convective-scale data assimilation investigations

Ruth Elizabeth Petrie[1,2], Ross Noel Bannister[1], and Michael John Priestley Cullen[3]

[1]Dept. of Meteorology, Univ. of Reading, Earley Gate, Reading, RG6 6BB, UK
[2]Now at The Centre for Environmental Data Analysis, RAL Space R25 - Room 1.22, STFC Rutherford Appleton Laboratory, Harwell Oxford, Didcot, OX11 0QX, UK
[3]Met Office, FitzRoy Road, Exeter, EX1 3PB, UK

Correspondence to: Ross Bannister, r.n.bannister@reading.ac.uk

Abstract. In developing methods for convective-scale data assimilation (DA) it is necessary to consider the full range of motions governed by the compressible Navier-Stokes equations (including non-hydrostatic and ageostrophic flow). These equations describe motion on a wide range of time-scales with non-linear coupling. For the purpose of developing new DA techniques that suit the convective-scale problem it is helpful to use so-called 'toy models' that are easy to run, and contain the same types of motion as the full equation set. Such a model needs to permit hydrostatic and geostrophic balance at the large-scales, but to allow imbalance at the small-scale, and in particular, they need to exhibit intermittent convection-like behaviour. Existing 'toy models' are not always sufficient for investigating these issues.

A simplified system of intermediate complexity derived from the Euler equations is presented, which support dispersive gravity and acoustic modes. In this system the separation of time scales can be greatly reduced by changing the physical parameters. Unlike in existing models, this allows the acoustic modes to be treated explicitly, and hence inexpensively. In addition, the non-linear coupling induced by the equation of state is simplified. This means that the gravity and acoustic modes are less coupled than in conventional models. A vertical slice formulation is used which contains only dry dynamics. The model is shown to give physically reasonabe results, and convective behaviour is generated by localised compressible effects. This model provides an affordable and flexible framework within which some of the complex issues of convective-scale DA can later be investigated. The model is called the "ABC model" after the three tunable parameters introduced: A (the gravity wave frequency), B (the modulation of the divergent term in the continuity equation), and C (defining the compressibility).

1 Introduction

Advances in computer power have enabled Numerical Weather Prediction (NWP) models to operate at higher resolutions than has previously been possible. In 2009 the Meteorological Office (Met Office) upgraded the resolution of its Unified Model (UM, Davies et al. (2005)) for the UK domain from $12\,\mathrm{km}$ to $1.5\,\mathrm{km}$ (Dixon et al., 2009). Resolutions of this degree are expected to resolve the large and synoptic scale features well. Bryan et al. (2003) found that models with resolutions of $100\,\mathrm{m}$ are necessary to provide meaningful simulations of convection. Resolutions of $\mathcal{O}(100\,\mathrm{m})$ are not yet affordable over the UK domain with current computer resources, although research experiments with the UM over smaller domains with $200\,\mathrm{m}$

Geosci. Model Dev. Discuss., doi:10.5194/gmd-2017-68, 2017
Manuscript under review for journal Geosci. Model Dev.
Discussion started: 25 April 2017
© Author(s) 2017. CC-BY 3.0 License.
Geoscientific Model Development Discussions

resolution have shown marked benefit (Lean et al., 2008). Models of $\mathcal{O}(\lesssim 1\,\mathrm{km})$ resolution are known as convective-scale models because they are capable of resolving some convection explicitly, thus do not require a full convection scheme. For instance it is possible to explicitly represent features such as thunderstorms $\mathcal{O}(10\,\mathrm{km})$ and Mesoscale Convective Systems (MCSs) $\mathcal{O}(10\text{-}100\,\mathrm{km})$, though not necessarily resolve their internal structure (e.g. Bryan et al. (2003); Clark et al. (2005); Lean et al. (2008)). Convective-scale forecasting can facilitate more accurate and earlier indications of extreme or hazardous weather, e.g. severe convection (Lean et al., 2008), which is of clear benefit.

As NWP moves towards the convective-scale so it is appropriate to examine the data assimilation (DA) scheme underpinning the forecast. The DA process combines meteorological data from a variety of sources including satellites, radar, weather stations, and radiosondes with a previous forecast (a background state) to produce an analysis. The NWP model is then integrated forward from the analysed state. The DA scheme that combines the observed and background data should provide an analysis that is approximately consistent with the observations and the model. The development of our toy model is a step towards a detailed and technical investigation of the convective-scale DA problem though its utility is not limited to this application.

Convective-scale DA introduces new issues. The errors in the larger-scale flow are still present, but in addition there will be errors on the small scales resolved by the convective-scale model which will have a different correlation structure. A pragmatic solution is to rely on a larger scale DA system to correct the large-scale errors, and thus allow convective-scale DA to focus on small scales. The model introduced in this paper is intended to allow development of methods of assimilating information over all scales. Detailed reviews of the issues are given by Park and Županski (2003); Dance (2004); Sun (2005); Lorenc and Payne (2007).

The current Met Office operational large-scale DA scheme enforces hydrostatic balance as a strong constraint and exploits geostrophy as a weak constraint in the background error covariance model (Lorenc et al., 2000; Bannister, 2008). The use of the hydrostatic balance relationship is valid for flows where the aspect ratio is much less than one, e.g. Holton (2004); Vallis (2006). In regions of convection the aspect ratio increases and so hydrostatic balance may no longer be a good approximation. Vetra-Carvalho et al. (2012) demonstrated that hydrostatic balance breaks down in the UM when it is run at $1.5\,\mathrm{km}$ horizontal resolution in regions of convection. At mid and high latitudes the geostrophic assumption is accurate for large-scale flows where the Rossby number is small (e.g. Holton (2004)). At the convective-scale the Rossby number is not small and therefore the use of geostrophic balance is no longer appropriate. It is therefore important that these balances are relaxed in convective-scale DA. Some variational DA methods, such as those termed "EnsVar" (Lorenc, 2013; Liu and Xue, 2016; Bannister, 2017) use information from an ensemble to represent background error covariance information without, in principle, the need to impose balances via a prescribed background error covariance matrix. These methods though suffer from noise in the sampled error covariance matrix and so rely on fixes such as localisation, which is known to destroy balances when they are relevant (Kepert, 2009; Bannister, 2015). The sampled (and localised) error covariance matrix in these methods is often hybridised with a prescribed background error covariance matrix (Clayton et al., 2013), which does impose balances. This brings attention back to the validity of such balances when such methods are applied at convective-scales, and hence to simplified systems where this issue can be studied closely.

Geosci. Model Dev. Discuss., doi:10.5194/gmd-2017-68, 2017
Manuscript under review for journal Geosci. Model Dev.
Discussion started: 25 April 2017
© Author(s) 2017. CC-BY 3.0 License.

Operational systems have to resolve features at both the synoptic and the convective-scales, requiring a large number of grid points. Such systems are very expensive to run and are not ideal tools for research purposes. The wide range of time-scales means that semi-implicit integration schemes are required for efficiency, e.g. Davies et al. (2005), and the nonlinear coupling between acoustic and gravity waves through the equation of state makes analysing the small-scale behaviour difficult, (Thuburn et al., 2002). Thus it would be useful to have a simplified model which describes a variety of regimes but without the extreme separation of time-scales and the full nonlinear coupling between acoustic and gravity waves present in the real system. A simplified system that has these properties allows problems such as the convective-scale DA problem to be explored in a practical but physically realistic way.

Perhaps the simplest non-linear model of convection is the well-known Lorenz 63 system (Lorenz, 1963), which describes convection with only three variables. These are (respectively) proportional to the strength of the convective motion, the size of the temperature differences between the up- and down-welling air, and the degree of deviation from linearity of the temperature profile. The resulting three ordinary differential equations are easily integrated numerically, but they miss the representation of the complex spatial aspects of the problem required to mirror real forecasting problems. Würsch and Craig (2014) discuss the lack of availability of suitable simplified models of convection for DA research, and they note that people have tended to run full NWP models for this purpose, but in idealised settings (see references in Würsch and Craig (2014) for examples). These models however remain complicated and expensive to run. Würsch and Craig (2014) developed a simplified model for purposes of convective-scale DA research. Their model is based on the one-dimensional shallow water model, modified to account for the phase transitions of cloud formation and precipitation – essential processes in the formation of cumulus convection. Although their model has shown to be very useful for this purpose, its one-dimensionality makes it impossible to tackle questions relating to the breakdown of hydrostatic balance, and to simulate our inability in practical situations to resolve vertical structures from observations.

The simplified system derived in this paper is intended to be run in vertical slice geometry (longitude/height), so that many fewer degrees of freedom are needed than in an operational three-dimensional system. The equations are modified so that the speed of the acoustic and gravity waves can be controlled, and so the normally large separations in time-scales can be reduced. The equation of state is also modified so that the degree of coupling between the acoustic and gravity waves is reduced. The modifications are designed so that energy is conserved in the equations, which is necessary for realistic behaviour. In order to study the dynamically-related breakdown of balance, no moisture is included, but intermittent convection-like behaviour is still seen (e.g. via gravity wave breaking). These simplifications permit large-scale balanced flows and sporadic small-scale non-hydrostatic flows (i.e. convection) to coexist within the framework of a simplified and practical model.

Section 2 provides a derivation of the toy model equations which are analysed in terms of a scale analysis and energy conservation properties. Section 3 describes the numerical implementation of the model. Section 4 provides a linear analysis of the equations. Section 5 shows the results of an idealized integration which illustrates how the model can be used to simulate different flow regimes. Section 6 provides a summary and some concluding remarks. Future work will exploit this model in testing different approaches to convective-scale DA, as piloted in Petrie (2012).

© Author(s) 2017. CC-BY 3.0 License.

2 Derivation of the model equations

The model is derived from the compressible 3-D Euler equations (1), see e.g. Holton (2004); Pielke (2001); Vallis (2006):

$$\frac{\partial \mathbf{u}}{\partial t} + \mathbf{u}\cdot\nabla\mathbf{u} + \frac{1}{\rho}\nabla p + g\mathbf{k} + f\mathbf{k}\times\mathbf{u} = 0, \tag{1a}$$

$$\frac{\partial \rho}{\partial t} + \nabla\cdot(\rho\mathbf{u}) = 0, \tag{1b}$$

$$\frac{\partial \theta}{\partial t} + \mathbf{u}\cdot\nabla\theta = 0, \tag{1c}$$

$$p = \rho R\left(\frac{p}{p_{00}}\right)^{\kappa}\theta. \tag{1d}$$

Equations (1a) are the momentum equations, where t is time, $\mathbf{u} = (u, v, w)$ comprises zonal (u), meridional (v) and vertical (w) components, p is pressure, g is the acceleration due to gravity and ρ is density. The f-plane assumption is made and $\mathbf{k}$ is the vertical unit vector. Equation (1b) is the compressible mass continuity equation. Equation (1c) is the adiabatic thermodynamic equation where θ is potential temperature. Equation (1d) is the equation of state where $p_{00} = 1000\text{hPa}$, $\kappa = R/c_p$ is a constant, with c_p the specific heat capacity at constant pressure and R the gas constant for dry air.

From this set of equations we wish to construct a toy model that has large-scale geostrophically and hydrostatically balanced flow, permits intermittent convective-like behaviour and is of practical use for investigating issues that arise in the convective-scale DA problem (e.g. that it is cheap to integrate).

2.1 Modifications to the 3-D Euler equations

In order to derive a model with the properties outlined above Eqs. (1) are modified in two stages. Firstly, a set of physically based approximations are made and secondly a set of 'toy model' simplifications are made. The latter set does not attempt to replicate the real system, rather they are intended to retain desired physical characteristics of the real system but simplify the computational implementation. In order to simplify the system it will be assumed that the model is periodic in the zonal direction and homogeneous in the meridional direction (i.e. the variables are functions of longitude, height, and time only).

2.1.1 Physically based modifications

The variables are decomposed such that they have a basic state and perturbation component as in e.g. Pielke (2001):

$$\Phi(x,z,t) = \Phi_0(z) + \Phi'(x,z,t). \tag{2}$$

Here Φ applies to any model variable except θ (for θ see below). The basic state (subscript 0) is a function of height only, and the perturbation (primed) is a function of longitude (x), height (z), and time (t). Potential temperature contains also a constant reference value (subscript R):

$$\theta(x,z,t) = \theta_{\mathrm{R}} + \theta_0(z) + \theta'(x,z,t). \tag{3}$$

Geosci. Model Dev. Discuss., doi:10.5194/gmd-2017-68, 2017
Manuscript under review for journal Geosci. Model Dev.
Discussion started: 25 April 2017
© Author(s) 2017. CC-BY 3.0 License.

The wind components u, v and w have zero reference state values, therefore the prime notation is dropped for the winds. For convenience, explicit reference to the arguments x and z will be dropped in much of the following derivation.

The basic state is assumed to satisfy hydrostatic balance

$$\frac{\partial p_0}{\partial z} = -\rho_0 g, \tag{4}$$

and the equation of state is

$$p_0 = \rho_0 R \left(\frac{p_0}{p_{00}}\right)^{\kappa} (\theta_\mathrm{R} + \theta_0). \tag{5}$$

The Brunt-Väisälä frequency, N, is defined as

$$N^2 = \frac{g}{\theta_\mathrm{R}} \frac{d\theta_0}{dz}. \tag{6}$$

The pressure gradient terms in Eq. (1a) are represented with Eq. (2), products of perturbations are neglected, and it is assumed that $\rho_0 \gg \rho'$ in the momentum equations. A buoyancy variable, $b = b_0(z) + b'(x,z)$, is introduced for convenience, it is related to θ by

$$b = b_0(z) + b' = \frac{g}{\theta_\mathrm{R}} \left(\theta_\mathrm{R} + \theta_0(z) + \theta'\right). \tag{7}$$

Combining these physically based approximations gives the following equations:

$$\frac{\partial u}{\partial t} + \mathbf{u}\cdot\nabla u + \frac{1}{\rho_0}\frac{\partial p'}{\partial x} - fv = 0, \tag{8a}$$

$$\frac{\partial v}{\partial t} + \mathbf{u}\cdot\nabla v + fu = 0, \tag{8b}$$

$$\frac{\partial w}{\partial t} + \mathbf{u}\cdot\nabla w + \frac{1}{\rho_0}\frac{\partial p'}{\partial z} + \frac{g}{\rho_0}\rho' = 0, \tag{8c}$$

$$\frac{\partial \rho'}{\partial t} + \nabla\cdot(\rho\mathbf{u}) = 0, \tag{8d}$$

$$\frac{\partial b'}{\partial t} + \mathbf{u}\cdot\nabla b' + N^2 w = 0, \tag{8e}$$

$$p = \rho R \left(\frac{p}{p_{00}}\right)^{\kappa} \theta, \tag{8f}$$

$$b' = \frac{g}{\theta_\mathrm{R}}\theta'. \tag{8g}$$

2.1.2 The “ABC model” modifications

It is desirable to reduce the stiffness of system Eqs. (8) so that it can be integrated explicitly with a time-step that is not too small. The following ‘toy model’ modifications are made so that the toy equations retain the basic properties desired, i.e. be geostrophically and hydrostatically balanced on the large-scale but permit intermittent convection-like behaviour on the small-scale that is unbalanced. The modifications are as follows.

Geosci. Model Dev. Discuss., doi:10.5194/gmd-2017-68, 2017
Manuscript under review for journal Geosci. Model Dev.
Discussion started: 25 April 2017
© Author(s) 2017. CC-BY 3.0 License.

1. We control the gravity waves by replacing N by the tunable parameter, A (which has units of s^{-1}). This is the pure gravity wave frequency (Sect. 4.3).

2. We control the acoustic waves by multiplying the divergent term of the compressible continuity equation by the dimensionless parameter B (where $0 < B \leq 1$). To ensure energy conservation (Sect. 2.3) it is required that B also multiplies the advective components of the momentum and thermodynamic equations. Acoustic waves can have frequencies that are normally much higher than gravity waves, but choosing a small B can help to reduce the acoustic wave frequencies.

The effect of these parameters on the wavespeeds will be demonstrated by numerical linear analysis in Sect. 4.5. The acoustic and gravity waves in the real atmosphere are coupled through the equation of state (Thuburn et al., 2002). This coupling can be reduced by using a linearized and simplified equation of state. Linearizing Eq. (8f) about the basic state gives

$$(1-\kappa)p_0^{-\kappa}p' = \frac{\rho' R\theta_{\mathrm{R}}}{p_{00}^{\kappa}} + \frac{\rho_0 R\theta'}{p_{00}^{\kappa}}, \tag{9}$$

where we have used $\theta_{\mathrm{R}} + \theta_0 \approx \theta_{\mathrm{R}}$. This is used in two ways to give modifications 3 and 4 below.

3. Firstly, for the purpose of relating density and buoyancy perturbations in Eq. (8c), we neglect pressure perturbations in Eq. (9):

$$\frac{\rho'}{\rho_0} = -\frac{\theta'}{\theta_{\mathrm{R}}}, \tag{10}$$

which by Eq. (8g) equals $-b'/g$.

4. Secondly and separately, for the purposes of simplifying the equation of state, neglecting buoyancy perturbations in the linearised equation of state Eq. (9) gives

$$(1-\kappa)p_0^{-\kappa}p' = \frac{\rho' R\theta_{\mathrm{R}}}{p_{00}^{\kappa}}. \tag{11}$$

This is a means of decoupling gravity and acoustic waves. Further, setting

$$C = \frac{R\theta_{\mathrm{R}}p_0^{\kappa}}{p_{00}^{\kappa}(1-\kappa)}, \tag{12}$$

gives the simplified equation of state

$$p' = C\rho', \tag{13}$$

where C is taken to be a global constant, and has units of $\mathrm{Nmkg}^{-1} = \mathrm{m}^2\mathrm{s}^{-2}$. The quantity $\sqrt{BC}$ is the pure sound wave speed in this system (Sect. 4.4).

5. Reference density ρ_0 is taken to be a constant and not a function of height.

6. Define the scaled density perturbation, $\tilde{\rho}'$ as

$$\tilde{\rho}' = \frac{\rho'}{\rho_0}, \tag{14}$$

and with this definition, $\tilde{\rho}_0 = 1$.

Geosci. Model Dev. Discuss., doi:10.5194/gmd-2017-68, 2017
Manuscript under review for journal Geosci. Model Dev.
Discussion started: 25 April 2017
© Author(s) 2017. CC-BY 3.0 License.

Combining modifications 1 to 6 gives the final form of the toy model equations:

$$\frac{\partial u}{\partial t} + B\mathbf{u}\cdot\nabla u + C\frac{\partial \tilde{\rho}'}{\partial x} - fv = 0, \tag{15a}$$

$$\frac{\partial v}{\partial t} + B\mathbf{u}\cdot\nabla v + fu = 0, \tag{15b}$$

$$\frac{\partial w}{\partial t} + B\mathbf{u}\cdot\nabla w + C\frac{\partial \tilde{\rho}'}{\partial z} - b' = 0, \tag{15c}$$

$$\frac{\partial \tilde{\rho}'}{\partial t} + B\nabla\cdot(\tilde{\rho}\mathbf{u}) = 0, \tag{15d}$$

$$\frac{\partial b'}{\partial t} + B\mathbf{u}\cdot\nabla b' + A^2 w = 0. \tag{15e}$$

Note that Eq. (15d) conserves mass following the flow modulated by B, i.e. $B\mathbf{u}$, but total mass remains conserved (Sect. 2.3.1). We also include the following tracer transport equation for diagnostic purposes:

$$\frac{\partial q}{\partial t} + \mathbf{u}\cdot\nabla q = 0, \tag{16}$$

where q is the tracer concentration. Note that the advection term is not multiplied by B in Eq. (16) (as B will be generally chosen as $B \leq 1$, we allow advection of the tracer to have its full effect so that tracer transport can be seen over an integration of a few hours). We refer to these simplified equations as the "ABC model" reflecting the three tunable parameters.

2.2 Scale analysis of the "ABC" model

A scale analysis of Eqs. (15) is performed by non-dimensionalising the equations using characteristic values. Our scale analysis deviates from standard analyses in two ways: (i) we allow different characteristic length-scales for each variable (in the horizontal and vertical), and (ii) we do not assume incompressibility (see below for more explanation of this). For the characteristic values we set $u = \mathcal{U}u^*$, $v = \mathcal{V}v^*$, $w = \mathcal{W}w^*$, $\tilde{\rho}' = \mathcal{P}'\tilde{\rho}'^*$, $\tilde{\rho} \sim 1$, and $b' = \mathcal{B}b'^*$. For the characteristic horizontal length-scales we set (respectively for each variable) $x = \mathcal{L}_u^{\mathrm{H}} x_u^*$, $x = \mathcal{L}_v^{\mathrm{H}} x_v^*$, $x = \mathcal{L}_w^{\mathrm{H}} x_w^*$, $x = \mathcal{L}_{\tilde{\rho}'}^{\mathrm{H}} x_{\tilde{\rho}'}^*$ and $x = \mathcal{L}_{b'}^{\mathrm{H}} x_{b'}^*$, and for the vertical length-scales $z = \mathcal{L}_u^{\mathrm{V}} z_u^*$, $z = \mathcal{L}_v^{\mathrm{V}} z_v^*$, $z = \mathcal{L}_w^{\mathrm{V}} z_w^*$, $z = \mathcal{L}_{\tilde{\rho}'}^{\mathrm{V}} z_{\tilde{\rho}'}^*$ and $z = \mathcal{L}_{b'}^{\mathrm{V}} z_{b'}^*$. The timescale is set as $t = \left[\mathcal{L}_u^{\mathrm{H}}/(B\mathcal{U})\right] t^*$. Upper case calligraphic variables (except $\mathcal{L}$) are characteristic values, starred variables are non-dimensional and $\mathcal{O}(1)$, and $\mathcal{L}_p^{\mathrm{H/V}}$ represents the horizontal/vertical length-scale of variable p.

Often in scale analyses the characteristic vertical speed, $\mathcal{W}$, is written in terms of other characteristic variables by using the incompressible continuity equation in a 2-D (longitude-height) system $\partial u/\partial x + \partial w/\partial z = 0$. Scaling this gives $\mathcal{W} \sim \mathcal{U}\mathcal{L}_w^{\mathrm{V}}/\mathcal{L}_u^{\mathrm{H}}$. We do not use this relation as some of the flows considered are highly compressible.

Using these definitions in Eqs. (15) and introducing the Rossby number, $Ro = \mathcal{U}/f\mathcal{L}_u^{\mathrm{H}}$, the aspect ratio, $\mathcal{A} = \mathcal{L}_u^{\mathrm{V}}/\mathcal{L}_u^{\mathrm{H}}$, the vertical-to-zonal wind ratio, $\mathcal{W}_{\mathcal{U}} = \mathcal{W}/\mathcal{U}$, and the meridional-to-zonal wind ratio, $\mathcal{V}_{\mathcal{U}} = \mathcal{V}/\mathcal{U}$ gives the following non-

Geosci. Model Dev. Discuss., doi:10.5194/gmd-2017-68, 2017
Manuscript under review for journal Geosci. Model Dev.
Discussion started: 25 April 2017
© Author(s) 2017. CC-BY 3.0 License.
Geoscientific Model Development Discussions
Open Access EGU

dimensionalised equations:

$$BRo\left[\frac{\partial u^*}{\partial t^*}+u^*\frac{\partial u^*}{\partial x^*_u}+\mathcal{A}^{-1}\mathcal{W}_\mathcal{U}w^*\frac{\partial u^*}{\partial z^*_u}\right]+\frac{C\mathcal{P}'}{\mathcal{U}f\mathcal{L}^{\mathrm{H}}_{\tilde{\rho}'}}\frac{\partial\tilde{\rho}'^*}{\partial x^*_{\tilde{\rho}'}}-\mathcal{V}_\mathcal{U}v^* = 0, \tag{17a}$$

$$BRo\left[\frac{\partial v^*}{\partial t^*}+\frac{\mathcal{L}^{\mathrm{H}}_u}{\mathcal{L}^{\mathrm{H}}_v}u^*\frac{\partial v^*}{\partial x^*_v}+\frac{\mathcal{L}^{\mathrm{H}}_u}{\mathcal{L}^{\mathrm{V}}_v}\mathcal{W}_\mathcal{U}w^*\frac{\partial v^*}{\partial z^*_v}\right]+\mathcal{V}_\mathcal{U}^{-1}u^* = 0, \tag{17b}$$

$$BRo\left[\frac{\partial w^*}{\partial t^*}+\frac{\mathcal{L}^{\mathrm{H}}_u}{\mathcal{L}^{\mathrm{H}}_w}\frac{\partial w^*}{\partial x^*_w}+\frac{\mathcal{L}^{\mathrm{H}}_u}{\mathcal{L}^{\mathrm{V}}_w}\mathcal{W}_\mathcal{U}w^*\frac{\partial w^*}{\partial z^*_w}\right]+\frac{C\mathcal{P}'}{\mathcal{W}f\mathcal{L}^{\mathrm{V}}_{\tilde{\rho}'}}\frac{\partial\tilde{\rho}'^*}{\partial z^*_{\tilde{\rho}'}}-\frac{\mathcal{B}'}{\mathcal{W}f}b'^* = 0, \tag{17c}$$

$$\frac{\partial\tilde{\rho}'^*}{\partial t^*}+\frac{\partial\tilde{\rho}^*u^*}{\partial x^*_u}+\frac{\mathcal{L}^{\mathrm{H}}_u}{\mathcal{L}^{\mathrm{V}}_w}\mathcal{W}_\mathcal{U}\frac{\partial\tilde{\rho}^*w^*}{\partial z^*_w} = 0, \tag{17d}$$

$$BRo\left[\frac{\partial b'^*}{\partial t^*}+\frac{\mathcal{L}^{\mathrm{H}}_u}{\mathcal{L}^{\mathrm{H}}_{b'}}u^*\frac{\partial b'^*}{\partial x^*_{b'}}+\frac{\mathcal{L}^{\mathrm{H}}_u}{\mathcal{L}^{\mathrm{V}}_{b'}}\mathcal{W}_\mathcal{U}w^*\frac{\partial b'^*}{\partial z^*_{b'}}\right]+\frac{A^2\mathcal{W}}{\mathcal{B}'f}w^* = 0. \tag{17e}$$

When the first three terms of Eq. (17a) and Eq. (17b) are small (often achieved with small Ro) the geostrophic relationships emerge. Expressed back in terms of the dimensional variables they are

$$-fv+C\frac{\partial\tilde{\rho}'}{\partial x} = 0, \tag{18a}$$

$$u = 0. \tag{18b}$$

Under similar circumstances Eq. (17c) defines the hydrostatic relationship. Expressed back in terms of the dimensional variables it is

$$-b'+C\frac{\partial\tilde{\rho}'}{\partial z}=0. \tag{19}$$

2.3 Conservation of mass and energy

As the toy model equations (15) are no longer based on standard thermodynamics, we must demonstrate that they form a physically reasonable set. To this end we now show that they conserve mass and energy.

2.3.1 Conservation of mass

Multiplying the continuity equation, Eq. (15d), by the constant ρ_0 gives the equation for the evolution of density perturbations. Adding the zero valued term $\partial\rho_0/\partial t$ then produces the equation for the evolution of density: $\partial\rho/\partial t+B\nabla\cdot(\rho\mathbf{u})=0$. Since the model uses periodic boundary conditions zonally, and zero vertical wind conditions at the top and bottom boundaries (Sect. 3.2), the divergence theorem shows that the equations conserve mass, $\int\int dxdz(\partial\rho/\partial t)=0$.

2.3.2 A useful 'identity' used to demonstrate conservation of energy

Dividing the continuity equation shown in Sect. 2.3.1 by ρ_0 gives the equation for $\tilde{\rho}$ evolution: $\partial\tilde{\rho}/\partial t+B\nabla\cdot(\tilde{\rho}\mathbf{u})=0$. Using this equation and expanding $\partial(\tilde{\rho}\gamma)/\partial t+B\nabla\cdot(\tilde{\rho}\gamma\mathbf{u})$, for an arbitrary time and space varying scalar field γ, we find:

$$\frac{\partial(\tilde{\rho}\gamma)}{\partial t}+B\nabla\cdot(\tilde{\rho}\gamma\mathbf{u})=\tilde{\rho}\left(\frac{\partial\gamma}{\partial t}+B\mathbf{u}\cdot\nabla\gamma\right). \tag{20}$$

Equation (20) is treated as an identity in the forthcoming energy analysis.

Geosci. Model Dev. Discuss., doi:10.5194/gmd-2017-68, 2017
Manuscript under review for journal Geosci. Model Dev.
Discussion started: 25 April 2017
© Author(s) 2017. CC-BY 3.0 License.

2.3.3 Kinetic energy

Multiplying respectively the momentum equations, (15a) to (15c), by $\tilde{\rho}u$, $\tilde{\rho}v$ and $\tilde{\rho}w$ and using (20) with $\gamma = u^2/2$, $\gamma = v^2/2$ and $\gamma = w^2/2$ we find:

$$\frac{\partial}{\partial t}\left(\frac{1}{2}\tilde{\rho}u^2\right) + B\nabla\cdot\left(\frac{1}{2}\tilde{\rho}u^2\mathbf{u}\right) + C\tilde{\rho}u\frac{\partial\tilde{\rho}'}{\partial x} - \tilde{\rho}ufv = 0, \tag{21a}$$

$$\frac{\partial}{\partial t}\left(\frac{1}{2}\tilde{\rho}v^2\right) + B\nabla\cdot\left(\frac{1}{2}\tilde{\rho}v^2\mathbf{u}\right) + \tilde{\rho}vfu = 0, \tag{21b}$$

$$\frac{\partial}{\partial t}\left(\frac{1}{2}\tilde{\rho}w^2\right) + B\nabla\cdot\left(\frac{1}{2}\tilde{\rho}w^2\mathbf{u}\right) + C\tilde{\rho}w\frac{\partial\tilde{\rho}'}{\partial z} - \tilde{\rho}wb' = 0. \tag{21c}$$

We can write the perturbation kinetic energy, E_k, as

$$E_\mathrm{k} = \frac{\tilde{\rho}}{2}\left(u^2+v^2+w^2\right), \tag{22}$$

which allows the sum of Eq. (21a) to Eq. (21c) to be written

$$\frac{\partial}{\partial t}E_\mathrm{k} + B\nabla\cdot(E_\mathrm{k}\mathbf{u}) - \tilde{\rho}b'w + C\tilde{\rho}\mathbf{u}\cdot\nabla\tilde{\rho}' = 0. \tag{23}$$

2.3.4 Buoyant energy

Multiplying the thermodynamic equation (15e) by $\tilde{\rho}b'/A^2$ and using Eq. (20) with $\gamma = b'^2/(2A^2)$, we find

$$\frac{\partial}{\partial t}E_\mathrm{b} + B\nabla\cdot(E_\mathrm{b}\mathbf{u}) + \tilde{\rho}b'w = 0, \tag{24}$$

where the perturbation buoyant energy, E_b, is

$$E_\mathrm{b} = \frac{\tilde{\rho}b'^2}{2A^2}. \tag{25}$$

2.3.5 Elastic energy

Multiplying the continuity equation (15d) by $C\tilde{\rho}'/B$ we find

$$\frac{\partial}{\partial t}E_\mathrm{e} + C\tilde{\rho}'\nabla\cdot(\tilde{\rho}\mathbf{u}) = 0, \tag{26}$$

where the perturbation elastic energy, E_e, is

$$E_\mathrm{e} = \frac{C\tilde{\rho}'^2}{2B}. \tag{27}$$

2.3.6 Total combined energy and its conservation

Adding Eqs. (23), (24), and (26) shows that the combined energy, $E = E_\mathrm{k} + E_\mathrm{b} + E_\mathrm{e}$, satisfies

$$\frac{\partial E}{\partial t} + B\nabla\cdot((E_\mathrm{k}+E_\mathrm{b})\mathbf{u}) + C\nabla\cdot(\tilde{\rho}'\tilde{\rho}\mathbf{u}) = 0. \tag{28}$$

Geosci. Model Dev. Discuss., doi:10.5194/gmd-2017-68, 2017
Manuscript under review for journal Geosci. Model Dev.
Discussion started: 25 April 2017
© Author(s) 2017. CC-BY 3.0 License.
Geoscientific Model Development Discussions

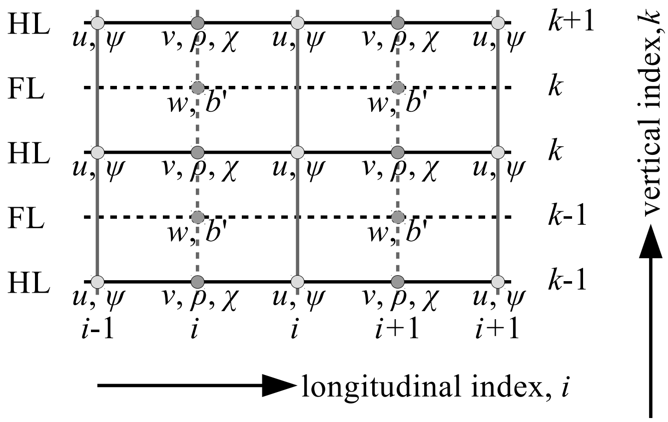

Figure 1. The arrangement of variables on the toy model's grid: an Arakawa-C grid in the horizontal and a Charney-Phillips grid in the vertical. Note the abbreviations: FL=Full Level and HL=Half Level.

Integrating Eq. (28) over the whole domain for the total combined energy gives

$$\int \frac{\partial E}{\partial t} dV + \int B\nabla \cdot ((E_{\mathrm{k}} + E_{\mathrm{b}})\mathbf{u}) dV + C \int \nabla \cdot (\tilde{\rho}' \tilde{\rho} \mathbf{u})\, dV = 0. \tag{29}$$

This toy model is set-up to have periodic boundary conditions in the x-direction, to have no variation in the y-direction, and to have zero vertical wind at the top and bottom boundaries (see Section 3.2). The divergence theorem then leads to conservation of total combined energy:

$$\frac{\partial}{\partial t}\left(\int E dV\right) = 0. \tag{30}$$

3 Numerical implementation of the "ABC model"

Now that a physically reasonable set of toy model equations has been formed, we now provide the details of how they are treated numerically.

3.1 Model discretization

The toy model uses a similar grid to that of the Southern UK (SUK) version of the UK Met Office's Unified Model (UM), but with some differences given below. In the horizontal the SUK model covers a domain of $540\,\mathrm{km}$ in longitude and $432\,\mathrm{km}$ in latitude with a resolution of $1.5\,\mathrm{km}$ on an Arakawa-C grid. In the vertical it has 70 vertical levels up to approximately $40\,\mathrm{km}$ on an irregularly spaced Charney-Philips grid (Lean et al., 2008).

The toy model grid is shown in Fig. 1. The differences from the SUK are that the toy model is periodic in the zonal direction, is homogeneous in the meridional direction, and uses regularly spaced vertical levels up to a lid of about $15\mathrm{km}$. The toy model uses only 60 levels (level spacing $\delta z \approx 250\,\mathrm{m}$) and has flat orography.

Geosci. Model Dev. Discuss., doi:10.5194/gmd-2017-68, 2017
Manuscript under review for journal Geosci. Model Dev.
Discussion started: 25 April 2017
© Author(s) 2017. CC-BY 3.0 License.
Geoscientific Model Development
Discussions

Table 1. Upper and lower boundary conditions of each prognostic model variable, z_0 is the the lower boundary and z_t is the upper boundary.

	Lower	Upper
u	$u(z_0) = 0$	$\frac{\partial u(z_t)}{\partial z} = 0$
v	$v(z_0) = 0$	$\frac{\partial v(z_t)}{\partial z} = 0$
w	$w(z_0) = 0$	$w(z_t) = 0$
$\tilde{\rho}'$	$\frac{\partial \tilde{\rho}'(z_0)}{\partial z} = 0$	$\frac{\partial \tilde{\rho}'(z_t)}{\partial z} = 0$
b'	$b'(z_0) = 0$	$b'(z_t) = 0$

This grid is a natural discretization of the equations which does not require a significant number of interpolations. There are approximately 10^5 variables in the state space of the toy system.

3.2 Boundary conditions

The vertical boundary conditions that we use are summarized in Table 1. At the lower boundary the horizontal winds are zero (no-slip conditions) and the vertical wind is zero to conserve total mass and energy. At the upper and lower boundaries the vertical derivative of density is zero. For the equations to have the capability to support hydrostatic balance, Eq. (19) implies that b' should be zero at the vertical boundaries. At the upper boundary the horizontal winds are chosen to maintain consistency with the boundary conditions of $\tilde{p}'$ and b' through thermal wind balance and the vertical wind is again zero to conserve total mass and energy.

3.3 Numerical differentiation and integration

3.3.1 Time integration scheme

The time integration is evaluated using a split explicit, forward-backward scheme (Cullen and Davies, 1991) and here we give a description of this scheme applied to Eqs. (15). The forward-backward scheme operates over a time-step Δt and comprises two stages: an adjustment stage and an advection stage.

Adjustment stage

The adjustment stage operates over a sub-timestep δt, where $\delta t = \delta t/n$ and n is typically a small positive integer (in this implementation $n = 2$). The adjustment stage contains two parts: the forward part and the backward part. Let t be the time at the start of the Δt timestep and let t_i be shorthand for $t + i\delta t$. The following is a description of the ith sub-timestep.

In the forward part of the forward-backward scheme, the momentum and thermodynamic equations are evaluated omitting the advective terms. The u and v equations are considered simultaneously to find the adjustment due to the Coriolis and pressure gradient terms. Then the w-momentum and b' equations are dealt with simultaneously to find the adjustment due to buoyancy,

Geosci. Model Dev. Discuss., doi:10.5194/gmd-2017-68, 2017
Manuscript under review for journal Geosci. Model Dev.
Discussion started: 25 April 2017
© Author(s) 2017. CC-BY 3.0 License.
Geoscientific Model Development Discussions

pressure gradient and vertical wind. The forward part of the adjustment stage gives an implicit approximation to u, v, w and b' at the next sub-timestep.

The equations for u Eq. (15a) and v Eq. (15b), omitting the advective terms are discretized as

$$u(t_{i+1}) = u(t_i) - \delta t C \frac{\partial \tilde{\rho}'(t_i)}{\partial x} + \frac{\delta t f}{2}\left(v(t_i) + v(t_{i+1})\right), \tag{31a}$$

$$v(t_{i+1}) = v(t_i) - \frac{\delta t f}{2}\left(u(t_i) + u(t_{i+1})\right). \tag{31b}$$

Solving Eqs. (31) for $u(t_{i+1})$ and $v(t_{i+1})$ gives

$$u(t_{i+1}) = \frac{\beta_f}{\alpha_f} u(t_i) - \frac{\delta t C}{\alpha_f}\frac{\partial \tilde{\rho}'(t_i)}{\partial x} + \frac{\delta t f}{\alpha_f} v(t_i), \tag{32a}$$

$$v(t_{i+1}) = \frac{\beta_f}{\alpha_f} v(t_i) - \frac{\delta t f}{\alpha_f} u(t_i) + \frac{\delta t^2 C f}{2\alpha_f}\frac{\partial \tilde{\rho}'(t_i)}{\partial x}, \tag{32b}$$

where α_f and β_f are defined by

$$\alpha_f = 1 + \frac{\delta t^2 f^2}{4}, \quad \text{and} \quad \beta_f = 1 - \frac{\delta t^2 f^2}{4}. \tag{33}$$

The equations for w Eq. (15c) and b' Eq. (15e) omitting advective terms are discretized as

$$w(t_{i+1}) = w(t_i) - \delta t C \frac{\partial \tilde{\rho}'(t_i)}{\partial z} + \frac{\delta t}{2}\left(b'(t_i) + b'(t_{i+1})\right), \tag{34a}$$

$$b'(t_{i+1}) = b'(t_i) - \frac{\delta t A^2}{2}\left(w(t_i) + w(t_{i+1})\right). \tag{34b}$$

Solving Eqs. (34) for $w(t_{i+1})$ and $b'(t_{i+1})$ gives

$$w(t_{i+1}) = \frac{\beta_A}{\alpha_A} w(t_i) - \frac{\delta t C}{\alpha_A}\frac{\partial \tilde{\rho}'(t_i)}{\partial z} + \frac{\delta t}{\alpha_A} b'(t_i), \tag{35a}$$

$$b'(t_{i+1}) = \frac{\beta_A}{\alpha_A} b'(t_i) - \frac{\delta t A^2}{\alpha_A} w(t_i) + \frac{\delta t^2 C A^2}{2\alpha_A}\frac{\partial \tilde{\rho}'(t_i)}{\partial z}, \tag{35b}$$

where α_A and β_A are defined by

$$\alpha_A = 1 + \frac{\delta t^2 A^2}{4}, \quad \text{and} \quad \beta_A = 1 - \frac{\delta t^2 A^2}{4}. \tag{36}$$

Equations (32a), (32b), (35a) and (35b) are the discretized forms of the split-explicit equations that are evaluated in the forward part of the forward-backward scheme in the adjustment stage. The spatial derivatives are left in continuous form, but are discretized in the numerics using standard centred finite-differences.

In the backward part of the forward-backward scheme the continuity equation (15d) is evaluated using the wind and buoyancy data calculated in the forward part, i.e.

$$\tilde{\rho}'(t_{i+1}) = \tilde{\rho}'(t_i) - \delta t B\left(\tilde{\rho}(t_i)\nabla\cdot\mathbf{u}(t_{i+1}) + \mathbf{u}(t_{i+1})\cdot\nabla\tilde{\rho}(t_i)\right). \tag{37}$$

The term in brackets on the right hand side is equal to $\nabla\cdot(\tilde{\rho}(t_i)\mathbf{u}(t_{i+1}))$, but has been expanded in Eq. (37) to allow the second term to use the upstream gradient of $\tilde{\rho}(t_i)$. After integration of n steps over the full Δt the value of $\tilde{\rho}'$ is known and the values of the variables u, v, w and b' are known but without the effect of advection.

© Author(s) 2017. CC-BY 3.0 License.

Advection stage

The advection stage advects the fields u, v, w and b' calculated in the adjustment stage using the sub-timestep-averaged winds $\bar{u}$ and $\bar{w}$, which are taken to be valid over the full Δt. Let ϕ be any of u, v, w or b', then the advection step is given by

$$\phi(t+\Delta t) = \phi(t) - \Delta t B \bar{\mathbf{u}} \cdot \nabla\phi(t), \tag{38}$$

where $\bar{\mathbf{u}} = (\bar{u}, \bar{w})^{\mathrm{T}}$. As with Eq. (37), the upwind gradient of ϕ is computed in Eq. (38). Note that for the tracer advection, $\phi = q$, Eq. (38) is used with $B = 1$.

Overall properties

The spatial derivatives evaluated by the forward-upstream scheme are first order accurate (Press et al., 2007) and the time integration which utilises a split-explicit and forward-backward scheme is also first-order accurate (Ames, 1958; Gadd, 1978). The stability of the forward-backward scheme increases the time-steps which are permitted by the CFL criterion (Ames, 1958). The split-explicit scheme has been used in early implementations of the UK Met Office's NWP model due to its ability to conserve mass (Gadd, 1978; Cullen and Davies, 1991).

4 Linear analysis of the "ABC model"

In this section a normal mode analysis of the toy model equations is performed. This follows a similar procedure used for the shallow water equations in Section 6.4 of Daley (1991) and in Section 2.4 of Cullen (2006). The linear analysis allows us to probe the dispersion relations and the balanced/unbalanced character of the linear modes. For simplicity this analysis is performed on a continuous domain of size L_x and L_z.

4.1 Linearisation

The non-linear model equations (15) are linearized about the reference state and a state of rest. It is convenient to write the model equations in terms of velocity potential, χ, and streamfunction, ψ. The Helmholtz theorem gives: $u = \partial\chi/\partial x$ and $v = \partial\psi/\partial x$. The linearized model equations are then:

$$\frac{\partial}{\partial t}\frac{\partial^2 \chi}{\partial x^2} + C\frac{\partial^2 \tilde{\rho}'}{\partial x^2} - f\frac{\partial^2 \psi}{\partial x^2} = 0, \tag{39a}$$

$$\frac{\partial}{\partial t}\frac{\partial^2 \psi}{\partial x^2} + f\frac{\partial^2 \chi}{\partial x^2} = 0, \tag{39b}$$

$$\frac{\partial w}{\partial t} + C\frac{\partial \tilde{\rho}'}{\partial z} - b' = 0, \tag{39c}$$

$$\frac{\partial \tilde{\rho}'}{\partial t} + B\frac{\partial^2 \chi}{\partial x^2} + B\frac{\partial w}{\partial z} = 0, \tag{39d}$$

$$\frac{\partial b'}{\partial t} + A^2 w = 0, \tag{39e}$$

Geosci. Model Dev. Discuss., doi:10.5194/gmd-2017-68, 2017
Manuscript under review for journal Geosci. Model Dev.
Discussion started: 25 April 2017
© Author(s) 2017. CC-BY 3.0 License.
Geoscientific Model Development Discussions
Open Access
EGU

Now take the following functional dependence for a particular dimensionless frequency σ, horizontal wavenumber k and vertical wavenumber m:

$$\left|\begin{array}{c} \chi(x,z,t) \\ \psi(x,z,t) \\ w(x,z,t) \\ \tilde{\rho}'(x,z,t) \\ b'(x,z,t) \end{array}\right| = \left|\begin{array}{cc} i & \hat{\chi} \\ 1 & \hat{\psi} \\ k/L_x & \hat{w} \\ k/L_x\sqrt{B/C} & \hat{\tilde{\rho}}' \\ -iAk/L_x & \hat{b}' \end{array}\right| \exp\left[i\left\{\left(\frac{kx}{L_x}\right)+\left(\frac{mz}{L_z}\right)-\sigma t\right\}\right]. \tag{40}$$

Substituting Eq. (40) into Eq. (39) and expressing the resulting set of equations in matrix form gives:

$$(\mathbf{L}-\sigma\mathbf{I})\left|\begin{array}{c} \hat{\chi} \\ \hat{\psi} \\ \hat{w} \\ \hat{\tilde{\rho}}' \\ \hat{b}' \end{array}\right| = 0, \tag{41}$$

where

$$\mathbf{L} = \begin{pmatrix} 0 & f & 0 & -\frac{k\sqrt{BC}}{L_x} & 0 \\ f & 0 & 0 & 0 & 0 \\ 0 & 0 & 0 & \frac{m\sqrt{BC}}{L_z} & A \\ -\frac{k\sqrt{BC}}{L_x} & 0 & \frac{m\sqrt{BC}}{L_z} & 0 & 0 \\ 0 & 0 & A & 0 & 0 \end{pmatrix}. \tag{42}$$

This is an eigenvalue equation where $\mathbf{L}$ is a real and symmetric matrix (due to the choice of factors in Eq. (40)), and so will have real eigenvalues. For each distinct choice of horizontal and vertical wavenumber (k,m), $\mathbf{L}$ has five eigenvalues, denoted σ_{R}, σ_{g}, $\sigma_{\mathrm{g}'}$, σ_{a}, and $\sigma_{\mathrm{a}'}$ where

$$\sigma_{\mathrm{R}} = 0, \quad \sigma_{\mathrm{g}} = -\sigma_{\mathrm{g}'}, \quad \text{and} \quad \sigma_{\mathrm{a}} = -\sigma_{\mathrm{a}'}. \tag{43}$$

The three distinct modes are the Rossby-like mode (subscript "R"), two inertia gravity modes ("g" and "g′"), and two acoustic modes ("a" and "a′"). The algebraic form of the R mode is simple and is discussed in Sect. 4.2 below, but the forms of the remaining modes are very complicated and so are considered only firstly in 'pure' forms (Sects. 4.3 and 4.4) and then numerically in the wave speed analysis (Sect. 4.5).

Geosci. Model Dev. Discuss., doi:10.5194/gmd-2017-68, 2017
Manuscript under review for journal Geosci. Model Dev.
Discussion started: 25 April 2017
© Author(s) 2017. CC-BY 3.0 License.

4.2 The Rossby-like mode

The normalized R mode is

$$\begin{pmatrix} \hat{\chi} \\ \hat{\psi} \\ \hat{w} \\ \hat{\tilde{\rho}}' \\ \hat{b}' \end{pmatrix} = \frac{1}{\sqrt{K}} \begin{pmatrix} 0 \\ -\frac{A}{f}\frac{k}{m}\frac{L_z}{L_x} \\ 0 \\ -\frac{AL_z}{m\sqrt{BC}} \\ 1 \end{pmatrix}, \tag{44}$$

where $K = (AL_z[kBC + L_x f^2] + L_x^2 f^2 m^2 C)/(L_x^2 f^2 m^2 BC)$. This mode, as we shall show, supports geostrophic balance defined by Eqs. (18a) and (18b). Firstly, relation Eq. (18a) in terms of the variables defined in Eq. (40) and for wavenumber k is

$$\frac{k}{L_x}\sqrt{BC}\hat{\tilde{\rho}}' = f\hat{\psi}, \tag{45}$$

which is consistent with Eq. (44). Secondly, and trivially, relation (18b) is equivalent to $\partial\chi/\partial x = 0$, which is also consistent with Eq. (44). There is no vertical wind associated with the R mode. There remains a buoyancy component for this mode to support hydrostatic balance defined by Eq. (19). Relation (19) in terms of the variables defined in Eq. (40) and for wavenumbers k, m is

$$\frac{m\sqrt{BC}}{L_z}\hat{\tilde{\rho}}' = -A\hat{b}', \tag{46}$$

which is consistent with Eq. (44).

4.3 The pure gravity waves

Following Kalnay (2002) pure gravity waves can be investigated by neglecting rotation and pressure perturbations (by Eq. (13) density perturbations are therefore neglected too). We anticipate that the gravity waves will be sensitive to A given that A is related to the static stability parameter N (the Brunt-Väisälä frequency). Under these conditions, Eq. (42) has two eigenvalues, $\sigma_{\mathrm{g}} = A$ and $\sigma_{g'} = -A$, representing the pure gravity wave frequencies. In the limit of $A = 0$, no gravity waves are supported.

4.4 The pure acoustic waves

Following Kalnay (2002) pure acoustic waves can be investigated by neglecting rotation, gravitation, and stratification (i.e. set $f = 0$, $g = 0$, $A^2 = 0$, and $b' = 0$). Under these conditions, Eq. (42) has three eigenvalues, $\sigma = 0$ (which is an incompressible mode that does not interest us here), $\sigma_{\mathrm{g}} = \sqrt{BC}\sqrt{(k/L_x)^2 + (m/L_z)^2}$ and $\sigma_{g'} = -\sigma_g$, the latter two representing the pure acoustic wave frequencies. The pure acoustic wave speed in the horizontal (e.g.) is $\partial\sigma_g/\partial(\frac{k}{L_x})$, which becomes $\sqrt{BC}$ in the scall-scale limit. In the limit that $B = 0$ or $C = 0$, the system becomes incompressible and no acoustic waves are supported.

Geosci. Model Dev. Discuss., doi:10.5194/gmd-2017-68, 2017
Manuscript under review for journal Geosci. Model Dev.
Discussion started: 25 April 2017
© Author(s) 2017. CC-BY 3.0 License.

4.5 Wave speed analysis experiments

In sections 4.3 and 4.4, we demonstrated how the pure gravity and acoustic waves depend upon the parameters A, B and C. The analysis there was simplified (by explicitly neglecting processes that are not directy associated with gravity and acoustic waves respectively) in order to derive analytical expressions. Here we look at the gravity and acoustic wave speeds in a more detailed way without making the approximations made before. These reveal the normal modes of the linearised system Eqs. (39) (see e.g. Thuburn et al. (2002)), which now include rotation, gravitation, and stratification. We show how the wavespeeds behave in the linearised system, and as a function of wavenumber, and of parameter values. To reduce the stiffness of the system we would like the speeds of the gravity and acoustic modes to have value $\sim \mathcal{U}$ or $\sim \mathcal{V}$, the characteristic speeds of the horizontal wind components, and so the results of this subsection are important for choosing parameter values for suitable model runs.

The standard values of the parameters that we use for this section are: $A = 0.02\,\mathrm{s}^{-1}$ (estimated from a typical value of the Brunt-Väisälä frequency), $B = 1.0$, $C = 10^5\,\mathrm{m}^2\mathrm{s}^{-2}$ (estimated from initialising data), and $f = 10^{-4}\,\mathrm{s}^{-1}$, and for simplicity, periodicity is assumed in the x and z directions.

Figure 2 shows the horizontal group speeds for the gravity ($c_\mathrm{g} = \partial\sigma_\mathrm{g}/\partial k$, panel a) and acoustic ($c_\mathrm{a} = \partial\sigma_\mathrm{a}/\partial k$, panel b) waves as a function of the integer index, n_x (characterising the horizontal wavenumber $k = 2n_x\pi/L_x$) for a range of parameter values (the integer index, n_z, characterising the vertical wavenumber $m = 2n_z\pi/L_z$, is fixed at $n_z = 3$). Note that these k and m are slightly different from those used in Sects. 4.1 to 4.4.

Gravity waves in the approximated system are found to be stationary (Sect. 4.3), but gravity waves in the full system are not, see Fig. 2a. There is a strong sensitivity of c_g to A (larger A, faster gravity waves), and the fastest gravity waves have large horizontal, and large vertical scales (small n_x and n_z). The sensitivity of c_g to BC over the values tested is weak, but it is detectable at large vertical scales and over large and intermediate horizontal scales (not shown). In fact, c_g increases with BC at large horizontal scales, but decreases with BC at intermediate horizontal scales ($n_x \sim 75$), but, as stated above, this effect is very weak.

Acoustic waves in this system have different characteristics to the gravity waves in many respects. Acoustic waves are generally much faster, but their speed may be controlled via the strong sensitivity of c_a to BC, and the fastest acoustic waves have small horizontal, and small vertical scales (large n_x and n_z), see Fig 2b. It is at these small scales that the acoustic waves saturate to the value $\sqrt{BC}$ as found in Sect. 4.4. The sensitivity of c_a to A is weak for the smaller values of A tested, but moderate for the largest value of A tested (not shown).

The ability of the parameters A, B and C to change the speed of both the horizontal gravity and acoustic waves has been demonstrated in Fig. 2. The buoyancy frequency parameter A, primarily controls the gravity waves, and the product BC primarily controls the acoustic waves. The vertical gravity and acoustic wave speeds respond in a similar way to the parameters as the horizontal waves (not shown). In addition to modifying the acoustic wave speeds, B and C have other, separate effects – B slows advection round the domain, and C influences the hydrostatic and geostrophic balance relationships (see section 2.2). It is permissible to alter the value of only one or any combination of these parameters depending on the required result. These results are used in the next section to help choose suitable parameter values.

Geosci. Model Dev. Discuss., doi:10.5194/gmd-2017-68, 2017
Manuscript under review for journal Geosci. Model Dev.
Discussion started: 25 April 2017
© Author(s) 2017. CC-BY 3.0 License.

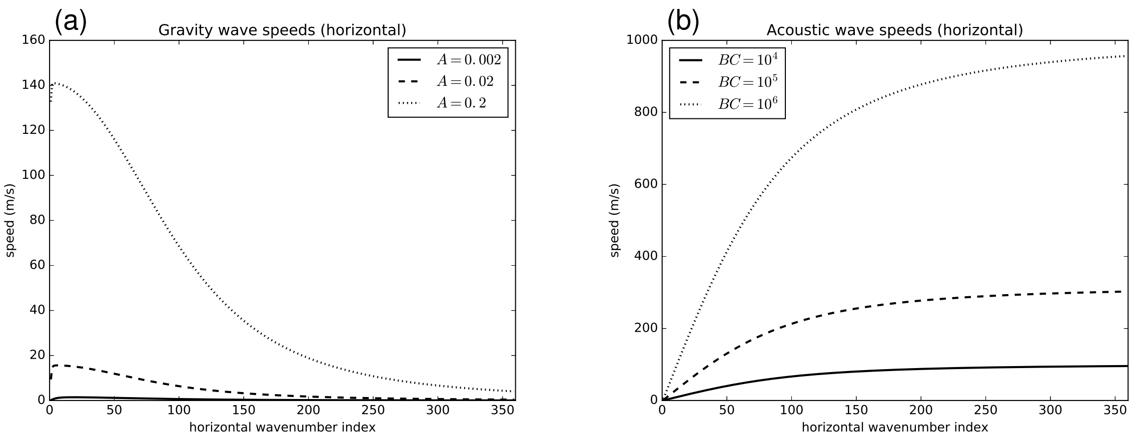

Figure 2. Panel (a) sensitivity of the horizontal gravity wave group speed to the tunable parameter A (in s^{-1}), where $BC = 10^5\,\mathrm{m}^2\mathrm{s}^{-2}$. Panel (b) sensitivity of the horizontal acoustic wave group speed to BC (in $\mathrm{m}^2\mathrm{s}^{-2}$), where $A = 0.02\,\mathrm{s}^{-1}$. In both panels $f = 10^{-4}\,\mathrm{s}^{-1}$ and the vertical wavenumber index is $n_z = 3$.

4.6 Reference parameters

In this section some desired dynamical characteristics that are seen in the real atmosphere are demonstrated in this simplified setup. It is required that the model mimics the multi-scale behaviour of the real atmosphere, i.e. displays hydrostatic and geostrophic balance on the large-scale while permitting imbalance and intermittent convective-like behaviour on the small-scale, while allowing an explicit solver. The results from the linear analysis of Sect. 4.5 gives a taste of how the wave speeds depend on A, B and C, but the values that we settle on as reference values are $A = 2\times10^{-2}\mathrm{s}^{-1}$, $B = 10^{-2}$ and $C = 10^4\mathrm{m}^2\mathrm{s}^{-2}$.

Figure 3a shows the frequencies, and the magnitudes of the horizontal and vertical wave speeds for the gravity and acoustic waves for these reference parameters. The acoustic wave frequencies in panel a are always higher than those of the gravity waves (the latter, have an upper bound of A). The frequencies of the gravity and acoustic waves for $n_z = 3$ (left) are of the same order, but for the extreme case of $n_z = 59$ (right), the acoustic wave frequencies have much higher values by more than an order of magnitude. These are classic dispersion curves for these modes in the atmosphere (e.g. Fig. 14.9 of Salby (1996)) and they allow us to estimate that the highest frequency that the model will encounter is $\sim 0.25\,\mathrm{s}^{-1}$ (4 s period, from the right panel of Fig. 3a). This allows us to set the time steps of our model (Sect. 3.3.1), which we chose as $\Delta t = 1\,\mathrm{s}$ and $\delta t = 0.5\,\mathrm{s}$.

The ability to control speeds in order to make the gravity and acoustic wave speeds comparable is more effective. Comparing, for instance, Figs. 3b and 2 shows how the gravity and acoustic wave speeds have been reduced to comparable values (a maximum of $10\,\mathrm{ms}^{-1}$ with the reference parameters, compared with a maximum of $1000\,\mathrm{ms}^{-1}$ for the parameters tested for Fig. 2). The speed of $10\,\mathrm{ms}^{-1}$ applies in the horizontal (Fig. 3b) and in the vertical (Fig. 3c). Given that the horizontal and vertical grid spacings are $1500\,\mathrm{m}$ and $250\,\mathrm{m}$ respectively, and $\Delta t = 1\,\mathrm{s}$, the Courant number is $Co = 1\times(10/1500 + 10/1500 + 10/250) \approx 0.05$, which is sufficiently small.

Geosci. Model Dev. Discuss., doi:10.5194/gmd-2017-68, 2017
Manuscript under review for journal Geosci. Model Dev.
Discussion started: 25 April 2017
© Author(s) 2017. CC-BY 3.0 License.
Geoscientific Model Development
Open Access
Discussions

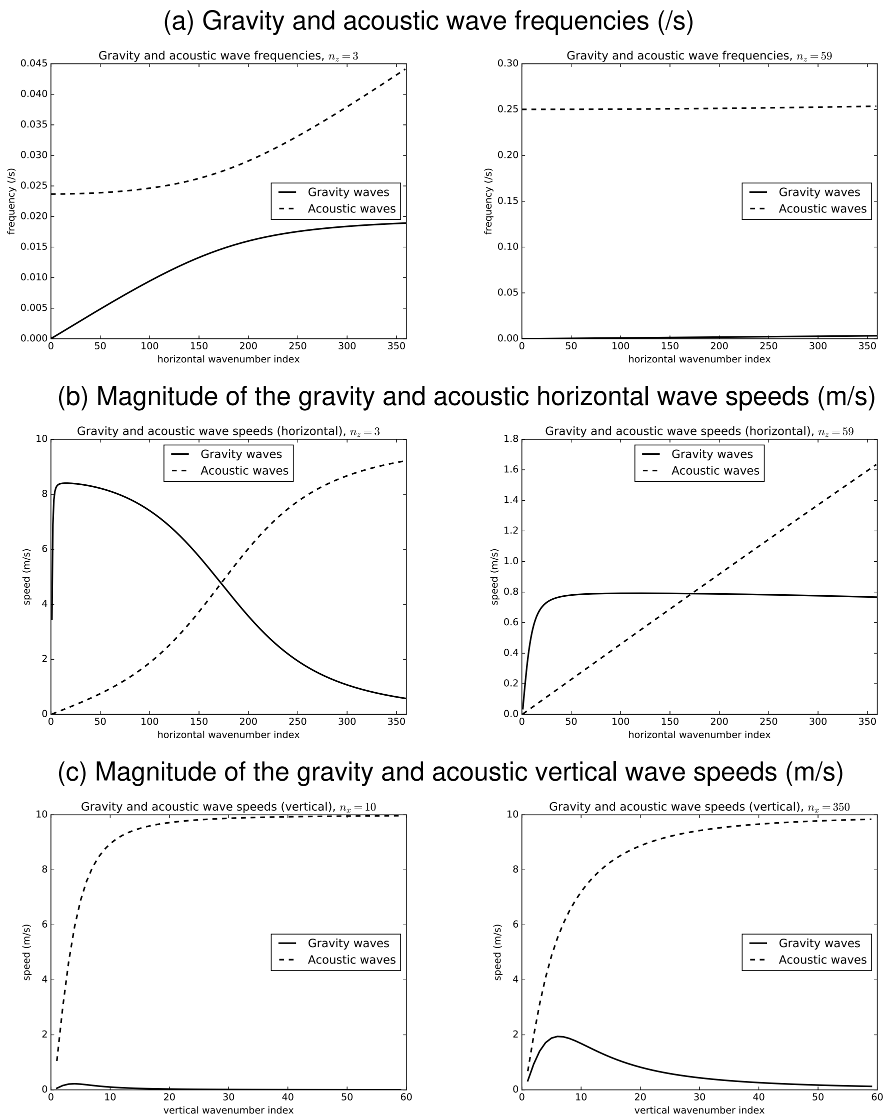

Figure 3. Gravity and acoustic wave properties for the reference parameters $A = 2 \times 10^{-2}\mathrm{s}^{-1}$, $B = 10^{-2}$ and $C = 10^4\mathrm{m}^2\mathrm{s}^{-2}$. The panels are: frequencies (a), and the magnitudes of the horizontal (b) and vertical (c) wave speeds. In (a) and (b) values are a function of horizontal wavenumber, n_x, and the left column is for $n_z = 3$, and the right column is for $n_z = 59$. In (c) values are a function of vertical wavenumber, n_z, and the left column is for $n_x = 10$, and the right column is for $n_x = 350$.

Geosci. Model Dev. Discuss., doi:10.5194/gmd-2017-68, 2017
Manuscript under review for journal Geosci. Model Dev.
Discussion started: 25 April 2017
© Author(s) 2017. CC-BY 3.0 License.

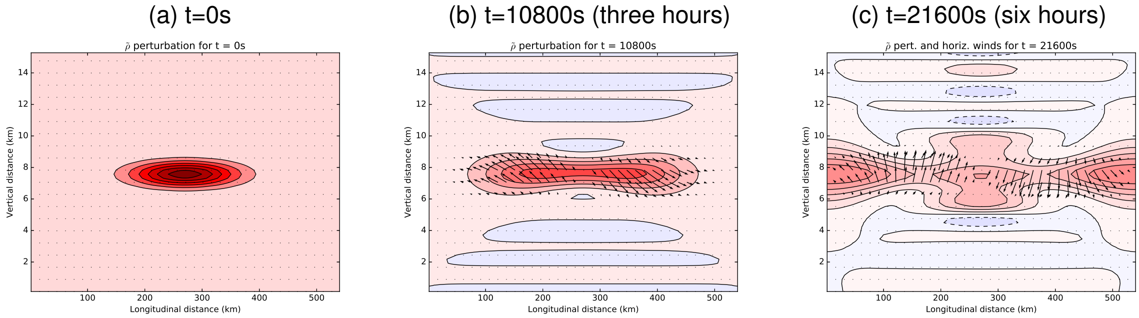

Figure 4. Model integration of the density perturbation $\tilde{\rho}'$, and horizontal wind vectors. The initial conditions are zero for all variables apart from $\tilde{\rho}'$, which takes the form of a Gaussian with an amplitude 0.01, a horizontal length-scale of $90\,\mathrm{km}$, and a vertical length-scale of $700\,\mathrm{m}$. The Gaussian is positioned in the middle of the domain. Parameters have the reference values $A = 2\times10^{-2}\,\mathrm{s}^{-1}$, $B = 10^{-2}$ and $C = 10^{4}\,\mathrm{m}^2\mathrm{s}^{-2}$. Note that the y-component of each wind arrow is the meridional, not the vertical, component of the wind. At six hours the maximum magnitude of the u-wind is $\sim 1.4\,\mathrm{ms}^{-1}$ and the maximum value of the v-wind is $\sim 3.6\,\mathrm{ms}^{-1}$.

5 "ABC model" integration results

5.1 Idealised initial conditions

The model was first initialised with idealised initial conditions to ensure that the model behaves reasonably with the reference parameter values. In this run the initial conditions are zero for all variables apart from $\tilde{\rho}'$, which takes the form of the Gaussian described in the caption (panel a). The $\tilde{\rho}'$ and (u, v) fields for up to six hours are shown in Fig. 4. In the real atmosphere such a positive density perturbation induces anticyclonic motion as geostrophic adjustment develops, and a similar response is seen in the toy model (the 'vertical' components of the arrows represent meridional wind, which is out of the page on the right and into the page on the left). After three hours (panel b), the horizontal wind is significantly divergent indicating that the $\tilde{\rho}'$ perturbation is being dissipated by gravity waves which act smooth-out the initial perturbation, whose maximum value has reduced to about a third of its original value. After six hours (panel c) the flow is mainly rotational (there is a weak convergent flow near the centre of the domain) and the $\tilde{\rho}'$ perturbation has moved to the boundaries.

Figure 4 can be used to verify the wave speeds determined by linear analysis. Consider Fig. 4b, where the edge of the feature has propagated approximately $80\,\mathrm{km}$ over the three hours. This gives an approximate horizontal gravity wave speed of $\sim 7\,\mathrm{ms}^{-1}$, which is around the maximum horizontal gravity wave speed found from the linear analysis in Fig. 3b.

5.2 Intermittent convection-like behaviour

Convective motion in the atmosphere is difficult to model and to assimilate as it is often intermittent and associated with small-scale divergence. In the real atmosphere it is usually driven by latent heating, but our simple model is dry and so we rely on other processes such as wave breaking to drive such motion. Intermittent convection-like motion is a desirable property of our

Geosci. Model Dev. Discuss., doi:10.5194/gmd-2017-68, 2017
Manuscript under review for journal Geosci. Model Dev.
Discussion started: 25 April 2017
© Author(s) 2017. CC-BY 3.0 License.
Geoscientific Model Development
Discussions

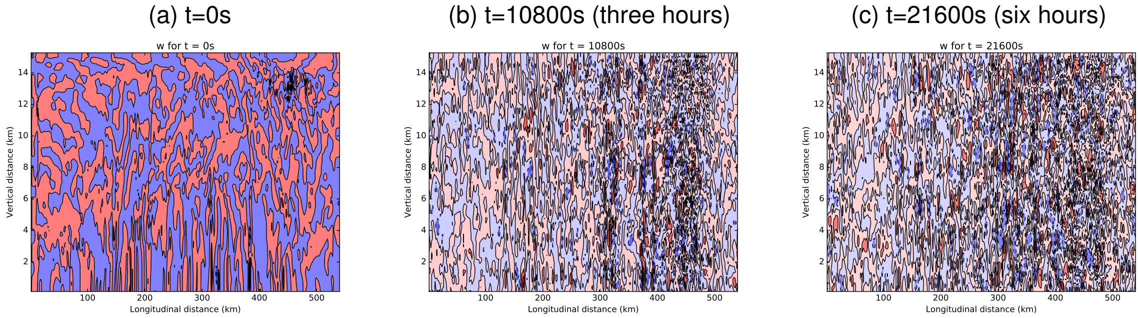

Figure 5. Model integration of the vertical wind w up to six hours. The initial conditions in panel a are derived from an output of the UM as described in the text (Sect. 5.2). Parameters have the reference values $A = 2\times10^{-2}\,\mathrm{s}^{-1}$, $B = 10^{-2}$ and $C = 10^{4}\,\mathrm{m}^2\mathrm{s}^{-2}$. At the initial time the maximum magnitude of w is $\sim 0.6\,\mathrm{ms}^{-1}$ and at six hours it is $\sim 0.16\,\mathrm{ms}^{-1}$.

model in order for it to have a significant unbalanced component on the small-scale, and hence be a useful system to study convective-scale data assimilation.

An obvious indication of the presence of convection is vertical motion and so we look at the w field from an integration of the model firstly with the reference parameters. The initial conditions of the model were created from the following procedure.

- Take values of u, v from a latitude/height slice of an output the Met Office's convective-scale ($1.5\mathrm{km}$ grid) UM (this is the same model used by the Met Office during the 2012 Olympics (Golding et al., 2014), and has the same horizontal resolution and grid staggering as our model). These fields are adjusted to eliminate the discontinuity imposed by the periodic boundary conditions[1].
- Calculate $\tilde{\rho}'$ by integrating the geostrophic balance equation (18a) on each level.
- Calculate b' from the hydrostatic balance equation (19) for each horizontal location.
- Calculate w from the continuity equation for zero three-dimensional divergence.

Each variable is then incremented (independently for each level) so that its horizontal mean is zero, and finally $\tilde{\rho}$ is set as $\tilde{\rho} = 1 + \tilde{\rho}'$. The model's initial conditions are then nearly balanced (the incrementing will disrupt the hydrostatic balance slightly), and unbalanced motion (including convection-like behaviour) then develops.

Figure 5 shows w over a six hour integration of the model using the reference parameters. The initial conditions in panel a show vertical winds that are of relatively small-scale in the horizontal, with elongated structures over the lowest $5\,\mathrm{km}$ or so in the middle of the domain. These are of course not generated by this model, but are derived from the UM data. An indication

[1]This is done by incrementing the left half of the domain by the amount $-((\Delta-\delta)/2)\exp\left[-(x/\ell)^2\right]$, and the right half by $+((\Delta-\delta)/2)\exp\left[-((x-L_x)/\ell)^2\right]$, where x is the horizontal distance from the western boundary, $\ell = 150\mathrm{km}$ is the relaxation distance, Δ is the size of the discontinuity in u or v (i.e. the magnitude of the difference in u or v between the western and eastern boundaries in the raw UM data), and δ is the magnitude of a typical increment of u or v between neighbouring grid-boxes. This procedure is performed separately for each vertical level.

Geosci. Model Dev. Discuss., doi:10.5194/gmd-2017-68, 2017
Manuscript under review for journal Geosci. Model Dev.
Discussion started: 25 April 2017
© Author(s) 2017. CC-BY 3.0 License.
Geoscientific Model Development Discussions

of the kind of behaviour that this model is capable of generating are shown in panels b and c, for three and six hours into the forecast respectively. The most striking aspect of the w field at three and six hours is that the scales of the features are even smaller than those at $t = 0$. Additionally the magnitudes of w are smaller with very small regions of moderate values especially in the eastern part of the domain. The similarity in these qualitative aspects of panels b and c shows that this kind of behaviour is not merely transient. We regard these plots as indicators of intermittent convection-like behaviour, which is studied further below.

5.3 Systematic exploration of model behaviour over parameter space

In order to test novel approaches to data assimilation it is desirable to run the model in different flow regimes, which we investigate by varying the parameters A, B, and C systematically, each over a three-hour model run. We are particularly interested in understanding how the parameter values affect the degree of convection and of imbalance, and we start this investigation by introducing the diagnostics for the reference parameters.

5.3.1 Reference parameters

We settle on four kinds of diagnostic for each parameter set, which are shown in Fig. 6 for the reference parameters. Panel a is the vertical wind speed, and panel b is the effective buoyancy, bu_{eff}. The latter is defined as the (non-constant) stability $bu_{\text{eff}} = \partial \left(b_0(z) + b'(x,z)\right)/\partial z$, where $\partial b_0(z)/\partial z = A^2$. A positive (negative) effective stability indicates statically (un)stable air, so negative and small positive values suggest convective activity. Panel c is the distribution of tracers after three hours. The tracers were initialised at $t = 0$ on a grid of 20 points distributed throughout the domain (dark regions) and the distribution after three hours provides an indication of the history of the wind behaviour. These fields are labeled with the minimum, maximum, and root-mean-squared values. Panel d indicates the degree of relative geostrophic imbalance (black lines and left scale) and hydrostatic imbalance (grey lines and right scale) averaged over the domain, at half-hour intervals over the integration. These quantities are found respectively using Eq. (18a) and Eq. (19) to give:

$$\text{geo. imbal} = \text{rms}\left[\left(C\frac{\partial\tilde{\rho}'}{\partial x} - fv\right) / \left(\text{rms}(C\partial\tilde{\rho}'/\partial x) + \text{rms}(fv)\right)\right], \tag{47a}$$

$$\text{hydro. imbal} = \text{rms}\left[\left(C\frac{\partial\tilde{\rho}'}{\partial z} - b'\right) / \left(\text{rms}(C\partial\tilde{\rho}'/\partial z) + \text{rms}(b')\right)\right], \tag{47b}$$

where rms indicates the root-mean-squared value of the quantity in brackets over the domain. The fields $\tilde{\rho}'$, v, and b' are filtered before computing these diagnostics by removing scales (i) below 100km (to give the solid lines in panel d), (ii) below 10km (to give the dashed lines), and (iii) below 1km (i.e. unfiltered, to give the dotted lines). This gives us an indication of how the degree of imbalance is affected by scale.

There are variations of upward and downward vertical motion over the domain (Fig. 6a), but there are no regions that are specifically more convectively active than others. The bu_{eff} diagnostic is fairly uniformly small over most of the domain (panel b) but does have more variability in the uppermost $5\,\text{km}$ of the domain where it is weakly negative in a thin layer at $14\,\text{km}$

Geosci. Model Dev. Discuss., doi:10.5194/gmd-2017-68, 2017
Manuscript under review for journal Geosci. Model Dev.
Discussion started: 25 April 2017
© Author(s) 2017. CC-BY 3.0 License.
Geoscientific Model Development
Discussions

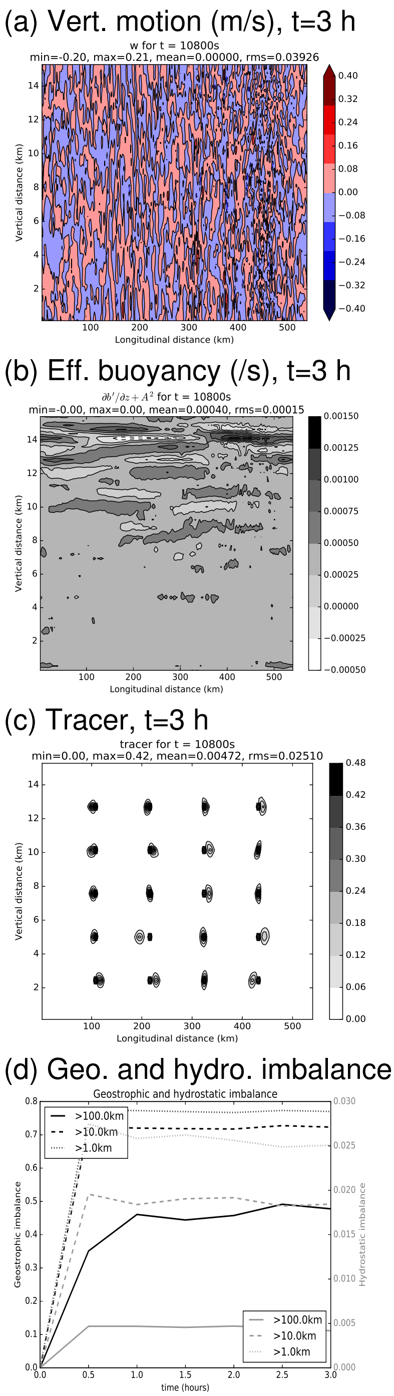

Figure 6. Selection of diagnostic fields for the reference parameters $A = 0.02\,\mathrm{s}^{-1}$, $B = 0.01$, $C = 10000\,\mathrm{m}^2\mathrm{s}^{-2}$. Panels (a-c) are after a three-hour forecast, except for the dark regions in (c), which indicate the tracer distribution at $t = 0$. In (d) the imbalances are shown as a function of forecast lead time and horizontal scale. The black lines (and the left scale) are for geostrophic imbalance, and the grey lines (and the right scale) are for hydrostatic imbalance. The Rossby number is estimated as $Ro \sim 0.06$.

Geosci. Model Dev. Discuss., doi:10.5194/gmd-2017-68, 2017
Manuscript under review for journal Geosci. Model Dev.
Discussion started: 25 April 2017
© Author(s) 2017. CC-BY 3.0 License.

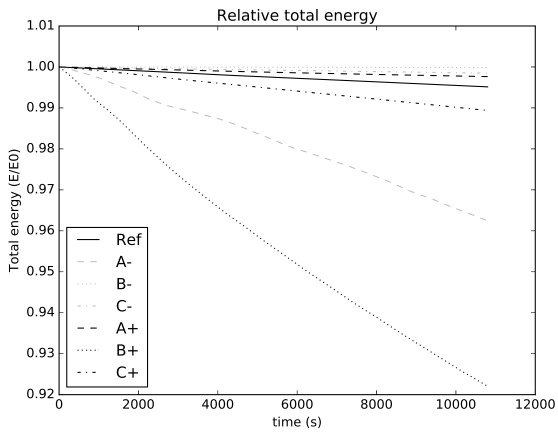

Figure 7. Relative total energy, $E(t)/E(0)$, from three-hour runs of the model with the reference parameters ("Ref"), and the six subsequent ways that the parameters were changed. The labels describe which parameter is modified in a model run and the + (-) indicates that it has been increased (decreased) by an order of magnitude from its reference value (with the remaining parameters unchanged).

(sandwiched between two strongly stable layers) during this snapshot. There is a small amount of disturbance of the tracer field after 3 hours (panel c).

The Rossby number is estimated to be small ($Ro \sim 0.06$), and the geostrophic imbalance is found to be moderate for the reference run (panel d), which stabilises to around 0.45 when only large scales are present, but higher, to around 0.7 to 0.8 when smaller scales are included (see the dark lines and the left-hand scale on panel d). The hydrostatic imbalance also increases as the scales shorten (see the light lines and the right-hand scale on panel d), but is much lower than the geostrophic imbalance (0.025 for the smallest scales). By estimating the magnitudes and length-scales of the fields in this run, the scale analysis in Sect. 2.2 does show that the last two terms in Eq. (17a) and in Eq. (17c) to be much larger than the other terms by about three and six orders of magnitude respectively.

Energy in the continuous system of equations was proven to be exactly conserved in Sect. 2.3, but the numerical integration scheme introduces errors which will lead to non-conservation. Fig. 7 (solid line) shows that these errors do lead to a small loss of energy over the three hours (less than half of a percent of the initial energy), which we assume is acceptable.

5.3.2 Changes to the parameter A

Recall that the parameter A controls the gravity wave frequency and speed. In this section two three-hour integrations are done: one with A decreased by an order of magnitude (A-, Fig. 8, left panels), and one with A increased by an order of magnitude (A+, Fig. 8, right panels).

A- appears to result in more active w values than in the reference run, and A+ appears to have little effect on w (panel a). The effective buoyancy (panel b) has more structure than in the reference run, with bands of lowered bu_{eff} appearing in A- (with patches of slightly negative bu_{eff} in the lower part of the domain which are too small to show as contours in the left plot

Geosci. Model Dev. Discuss., doi:10.5194/gmd-2017-68, 2017
Manuscript under review for journal Geosci. Model Dev.
Discussion started: 25 April 2017
© Author(s) 2017. CC-BY 3.0 License.

of panel b), while A+ has no negative values at all. The increased vertical motion in A- is seen in the tracer fields (panel c), which have been transported more vertically in A- and slightly less vertically in A+ than the reference run. These results make physical sense given that A controls the static stability of the fluid.

The geostrophic and hydrostatic imbalances for A- and the geostrophic imbalances for A+ (panel d) are similar to the reference run (slightly lower overall for A- and slightly higher for A+), but the hydrostatic imbalance diagnostic is up to four times higher for A+, although the imbalance is still small. These findings seem counter-intuitive (e.g. geostrophic imbalance may in fact be expected to increase as A is decreased as the separation between gravity and advective frequencies decreases). The result may be due to the rather arbitrary way that imbalance is defined in (47), although the computed Rossby number is found to remain around the same level in A- and A+ as the reference run[2]. The less statically stable A- run results in more numerical loss of energy than the reference run (4% loss over the three hours) (Fig. 7) and the more stable A+ run results in less loss of energy (0.2% loss).

5.3.3 Changes to the parameter B

Recall that the parameter B (with C) controls the acoustic wave speed. Two further three-hour integrations are done: one with B decreased by an order of magnitude (B-, Fig. 9, left panels), and one with B increased by an order of magnitude (B-, Fig. 9, right panels).

B- and B+ result in slightly more active w values, but little change to the structure of the w field (panel a). B+ does have more vertical motion in the root-mean-squared values than both the reference and B-. The effective buoyancy is largely unaffected by the changes in B (panel b). A similar story applies to the tracers for B-, but the tracers for B+ do show increased vertical transport (panel c), which is consistent with the larger root-mean-squared w for B+. The geostrophic and hydrostatic imbalances are slightly less for B-, but higher for B+, although the values remain small. The Rossby number is small for both runs ($Ro \sim 0.07$ for B-, but elevated $Ro \sim 0.11$ for B+). One would normally assume that a faster gravity wave speed, as in the B+ run, would result in less imbalance, but this is not the case here. The scale analysis in Sect. 2.2 reveals though that it is the product BRo, rather than just Ro that is the quantity that scales terms that knock the system out of balance, and BRo is smaller (larger) in B- (B+) than in the reference run. Changing the B parameter has a dramatic effect on errors in the energy conservation (Fig. 7), where B- produces the most conserved energy conservation of all experiments (the numerical loss of energy is indistinguishable from a perfectly conservative scheme in Fig. 7), but B+ results in one of the most erroneous runs (an eight percent loss in energy over three hours).

5.3.4 Changes to the parameter C

Recall that C is the parameter that conventionally controls the acoustic wave speed (in this system it controls it jointly with B). Two further three-hour integrations are done: one with C decreased by an order of magnitude (C-), and one with C increased

[2]Lowering A by a further order of magnitude from A- (i.e. $A = 0002\,\mathrm{s}^{-1}$, results not shown) does double the computed Rossby number though, which is more in line with expectation.

Geosci. Model Dev. Discuss., doi:10.5194/gmd-2017-68, 2017
Manuscript under review for journal Geosci. Model Dev.
Discussion started: 25 April 2017
© Author(s) 2017. CC-BY 3.0 License.
Geoscientific Model Development
Discussions
Open Access

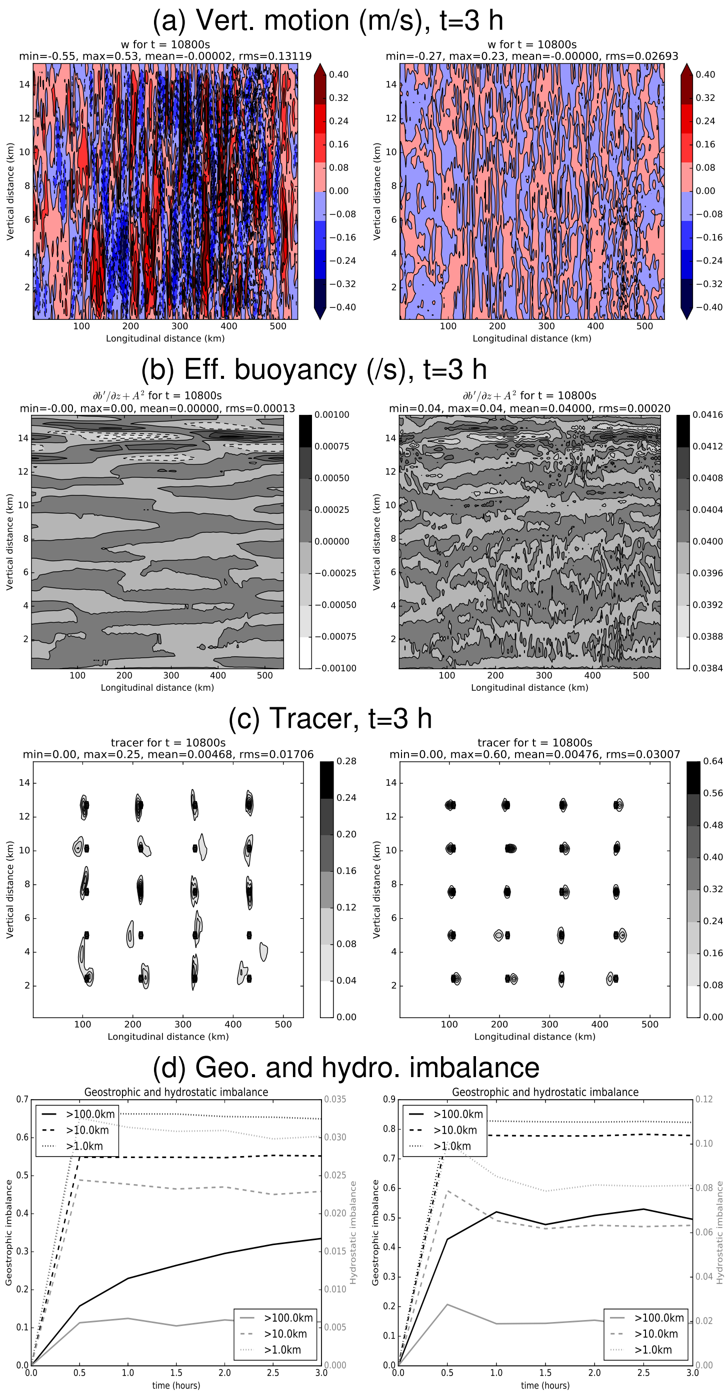

Figure 8. As Fig. 6 but for the modified A parameter: $A = 0.002\,\mathrm{s}^{-1}$ (A-, left panels, $Ro \sim 0.06$), and $A = 0.2\,\mathrm{s}^{-1}$ (A+, right panels, $Ro \sim 0.07$). The remaining parameters are as for the reference run ($B = 0.01$, $C = 10000\,\mathrm{m}^2\mathrm{s}^{-2}$).

Geosci. Model Dev. Discuss., doi:10.5194/gmd-2017-68, 2017
Manuscript under review for journal Geosci. Model Dev.
Discussion started: 25 April 2017
© Author(s) 2017. CC-BY 3.0 License.

Geoscientific Model Development Open Access Discussions EGU

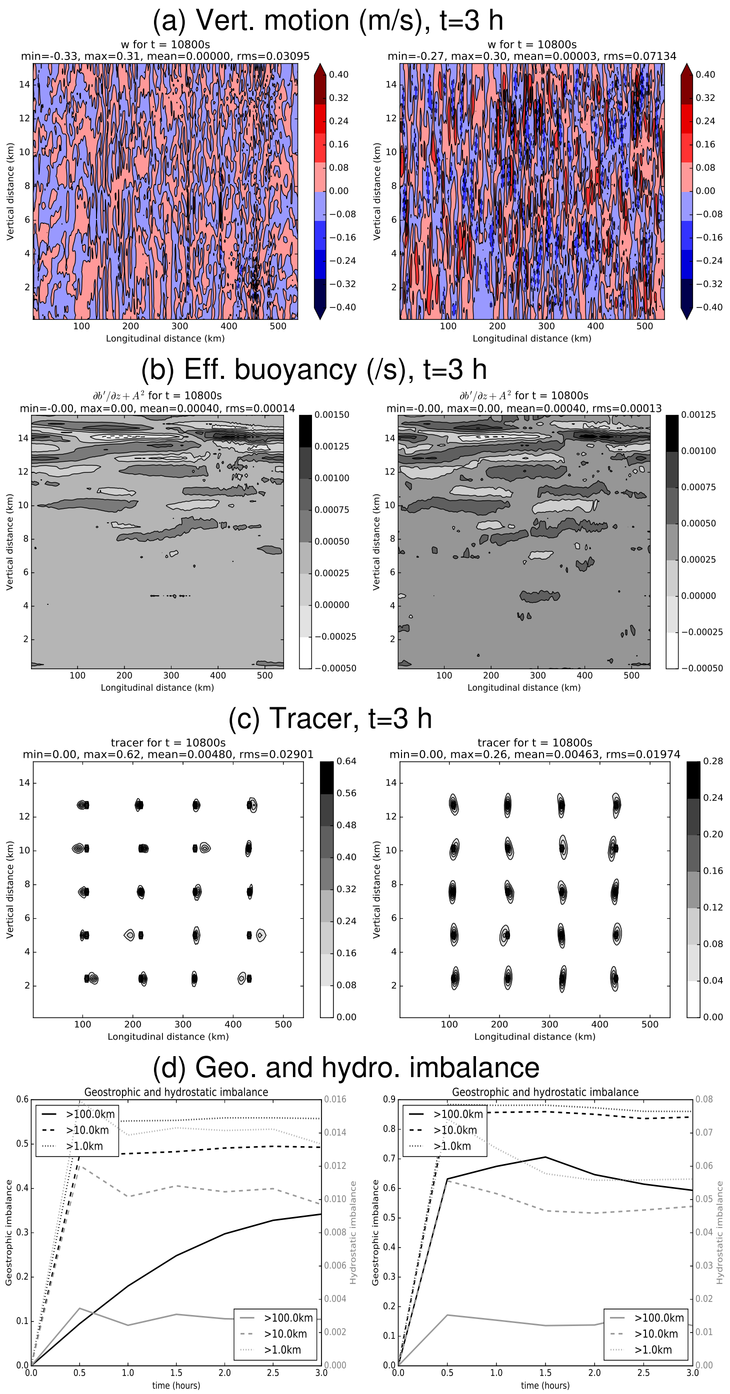

Figure 9. As Fig. 6 but for the modified B parameter: $B = 0.001$ (B-, left panels, $Ro \sim 0.07$), and $B = 0.1$ (B+, right panels, $Ro \sim 0.11$). The remaining parameters are as for the reference run ($A = 0.02\mathrm{s}^{-1}$, $C = 10000\mathrm{m}^2\mathrm{s}^{-2}$).

Geosci. Model Dev. Discuss., doi:10.5194/gmd-2017-68, 2017
Manuscript under review for journal Geosci. Model Dev.
Discussion started: 25 April 2017
© Author(s) 2017. CC-BY 3.0 License.

by an order of magnitude (C-). The initial conditions for C- and C+ each differ from those used before as the procedure used to generate balanced initial conditions described in Sect. 5.2 from UM data depends on parameter C.

The C- and C+ results are not shown because they are virtually indistinguishable from the B- and B+ runs respectively (including the relative balance results). There are two differences though. The first is that $\tilde{\rho}'$ is scaled by C^{-1} (when C is decreased (increased) by an order of magnitude, $\tilde{\rho}'$ (not shown) is increased (decreased) by an order of magnitude compared to the B- (B+) runs, with the field structures remaining the same). This is seen in the scale analysis equations (17), where C and $\mathcal{P}'$ (the characteristic value of $\tilde{\rho}'$) always appear together as a product. This is how the C- and C+ runs maintain the same level of geostrophic and hydrostatic balances as the B- and B+ runs respectively. The second difference is seen in the numerical scheme's energy loss (Fig. 7). The B+ run loses energy significantly (eight percent), but the C+ run loses less (one percent). This is another beneficial effect of introducing the B parameter (the same value of a particular desired acoustic wave speed $\sqrt{BC}$ can be achieved by decreasing B and increasing C).

6 Conclusions

A set of simplified energy conserving equations have been derived which allow control of the gravity and acoustic wave characteristics to be controlled with three parameters, A (the pure gravity wave frequency), B (the modulation of the divergent term in the continuity equation, and of the advection terms in other equations), and C (defining the compressibility of the system). The term $\sqrt{BC}$ is the pure small-scale acoustic wave speed. The introduction of B allows the acoustic wave speed to be reduced so that it is comparable to the gravity wave speed, hence allowing explicit integration schemes to be used to approximate the solution of the equation set (such as the split explicit, forward-backward scheme used here).

The linearised equations support a zero frequency Rossby-like mode and dispersive gravity and acoustic modes. The system is shown to behave in a way that reflects aspects of the atmosphere, namely geostrophic adjustment, convective behaviour influenced by buoyancy, and scale-dependent geostrophic and hydrostatic imbalances. The model has no water vapour, which simplifies the scheme considerable (although water vapour and moist processes could be added if required). The energy is not perfectly conserved with this scheme, although numerical energy loss is assumed to be acceptable in most runs.

The purpose of developing this model is to facilitate research into ways of modelling the background error covariance matrix ($\mathbf{B}$) used in convective-scale data assimilation. The $\mathbf{B}$-matrix is normally modelled with guidance from large-scale dynamics, namely that geostrophic balance is dominant, and hydrostatic balance is exact. These assumptions are probably not applicable at convective-scales (as shown by Berre (2000); Bannister et al. (2011); Vetra-Carvalho et al. (2012); Bannister (2015), and as we have seen here, where more imbalance is present at the smaller scales). A key idea which will be explored in a forthcoming paper is to use the normal mode structure of the linearised equations to define the $\mathbf{B}$-matrix rather than relying on imposed balances. It is hoped that this will have physically appropriate structures and the correct degree of balance at different scales (preliminary work has been done by Petrie (2012)).

© Author(s) 2017. CC-BY 3.0 License.

Geoscientific Model Development Discussions

7 Code and data availability

The model is written in Fortran-90, and the plotting code is written in python. This software is open-source and freely available on a Git Hub repository (Petrie et al., 2017). The initial conditions used to start the model runs studied in this paper is available from the same repository.

Author contributions. This work has emerged from the doctoral thesis of REP Petrie (2012). MJPC provided the main scientific guidance for the particular simplifications used to define the toy model, and REP did most of the coding and testing under the supervision of RNB. REP performed the initial model runs for her thesis, and RNB developed the code further and performed the model runs for this paper. This manuscript was drafted by REP, and RNB, with substantial advice from MJPC.

Competing interests. The authors declare that they have no conflict of interest.

Disclaimer.

Acknowledgements. REP was supported by a NERC/NCEO studentship for the course of this work, RNB is supported by the NCEO, and MJPC is supported by the Met Office. REP and RNB would like to thank the local assistance from Terry Davies, who helped REP code the integration scheme.

© Author(s) 2017. CC-BY 3.0 License.

References

Ames, W. F.: Numerical methods for partial differential equations, London, Nelson, 1958.

Bannister, R. N.: A review of forecast error covariance statistics in atmospheric variational data assimilation. II: Modelling the forecast error covariance statistics, Quarterly Journal of the Royal Meteorological Society, 134, 1971–1996, 2008.

Bannister, R. N.: How is the Balance of a Forecast Ensemble Affected by Adaptive and Nonadaptive Localization Schemes?, Mon. Wea. Rev., 143, 3680–3699, 2015.

Bannister, R. N.: A review of operational methods of variational and ensemble-variational data assimilation, Quarterly Journal of the Royal Meteorological Society, 143, 607–633, doi:DOI:10.1002/qj.2982, 2017.

Bannister, R. N., Migliorini, S., and Dixon, M.: Ensemble prediction for nowcasting with a convection-permitting model–II: forecast error statistics, Tellus A, 63, 497–512, 2011.

Berre, L.: Estimation of synoptic and mesoscale forecast error covariances in a limited-area model, Monthly weather review, 128, 644–667, 2000.

Bryan, G., Wyngaard, J., and Fritsch, J.: Resolution requirements for the simulation of deep moist convection, Mon. Wea. Rev., 131, 2394–2416, 2003.

Clark, P., Browning, K., and Wang, C.: The sting at the end of the tail: Model diagnostics of fine-scale three-dimensional structure of the cloud head, Quart. J. Roy. Meteor. Soc., 131, 2263–2292, 2005.

Clayton, A., Lorenc, A. C., and Barker, D. M.: Operational implementation of a hybrid ensemble/4D-Var global data assimilation system at the Met Office, Quart. J. Roy. Meteor. Soc., 139, 1445–1461, 2013.

Cullen, M. and Davies, T.: A conservative split-explicit integration scheme with fourth-order horizontal advection, Quarterly Journal of the Royal Meteorological Society, 117, 993–1002, 1991.

Cullen, M. J. P.: A mathematical theory of large-scale atmosphere/ocean flow, Imperial College Press, 2006.

Daley, R.: Atmospheric Data Analysis, Cambridge University Press, 1991.

Dance, S.: Issues in high resolution limited area data assimilation for quantitative precipitation forecasting, Physica D: Nonlinear Phenomena, 196, 1–27, 2004.

Davies, T., Cullen, M., Malcolm, A., Mawson, M., Staniforth, A., White, A., and Wood, N.: A new dynamical core for the Met Office's global and regional modelling of the atmosphere, Quarterly Journal of the Royal Meteorological Society, 131, 1759–1782, 2005.

Dixon, M., Li, Z., Lean, H., Roberts, N., and Ballard, S.: Impact of data assimilation on forecasting convection over the United Kingdom using a high-resolution version of the Met Office Unified Model, Monthly Weather Review, 137, 1562–1584, 2009.

Gadd, A. J.: A split explicit integration scheme for numerical weather prediction, Q. J. R. Meterol. Soc., 104, 569–582, 1978.

Golding, B., Ballard, S., Mylne, K., Roberts, N., Saulter, A., Wilson, C., Agnew, P., Davis, L., Trice, J., Jones, C., et al.: Forecasting capabilities for the London 2012 Olympics, Bulletin of the American Meteorological Society, 95, 883–896, 2014.

Holton, J.: An Introduction to Dynamic Meteorology, 4 edition, Academic Press, 2004.

Kalnay, E.: Atmospheric modeling, data assimilation and predictability, Cambridge University Press, 2002.

Kepert, J. D.: Covariance localisation and balance in an ensemble Kalman filter, Quarterly Journal of the Royal Meteorological Society, 135, 1157–1176, 2009.

Lean, H. W., Clark, P. A., Dixon, M., Roberts, N. M., Fitch, A., Forbes, R., and Halliwell, C.: Characteristics of high-resolution versions of the Met Office Unified Model for forecasting convection over the United Kingdom, Monthly Weather Review, 136, 3408–3424, 2008.

© Author(s) 2017. CC-BY 3.0 License.

Liu, C. and Xue, M.: Relationships among Four-Dimensional Hybrid Ensemble-Variational Data Assimilation Algorithms with Full and Approximate Ensemble Covariance Localization, Mon. Wea. Rev., 144, 591–606, 2016.

Lorenc, A., Ballard, S., Bell, R., Ingleby, N., Andrews, P., Barker, D., Bray, J., Clayton, A., Dalby, T., Li, D., et al.: The Met. Office global three-dimensional variational data assimilation scheme, Quarterly Journal of the Royal Meteorological Society, 126, 2991–3012, 2000.

Lorenc, A. C.: Recommended nomenclature for EnVar data assimilation methods, Research Activities in Atmospheric and Oceanic Modeling, WGNE, 2013.

Lorenc, A. C. and Payne, T.: 4D-Var and the butterfly effect: Statistical four-dimensional data assimilation for a wide range of scales, Quarterly Journal of the Royal Meteorological Society, 133, 607–614, 2007.

Lorenz, E. N.: Deterministic nonperiodic flow, Journal of the atmospheric sciences, 20, 130–141, 1963.

Park, S. K. and Županski, D.: Four-dimensional variational data assimilation for mesoscale and storm-scale applications, Meteorology and Atmospheric Physics, 82, 173–208, 2003.

Petrie, R. E.: Background error covariance modelling for convective-scale variational data assimilation, Ph.D. thesis, Univ. of Reading, Dept. of Meteorology, 2012.

Petrie, R. E., Bannister, R. N., and Cullen, M. J. P.: ABC model software, GitHub repository, doi:10.5281/zenodo.495405, 2017.

Pielke, R.: Mesoscale Meteorological Modeling, Academic Press, 2001.

Press, W., Teukolsky, S., Vetterling, W., and Flannery, B.: Numerical Recipes 3rd Edition: The Art of Scientific Computing, Cambridge University Press, 2007.

Salby, M. L.: Fundamentals of atmospheric physics, vol. 61, Academic press, 1996.

Sun, J.: Convective-scale assimilation of radar data: progress and challenges, Quarterly Journal of the Royal Meteorological Society, 131, 3439–3463, 2005.

Thuburn, J., Wood, N., and Staniforth, A.: Normal modes of deep atmospheres. I: Spherical geometry, Quarterly Journal of the Royal Meteorological Society, 128, 1771–1792, 2002.

Vallis, G.: Atmospheric and oceanic fluid dynamics, Cambridge University Press, 2006.

Vetra-Carvalho, S., Dixon, M., Migliorini, S., Nichols, N. K., and Ballard, S. P.: Breakdown of hydrostatic balance at convective scales in the forecast errors in the Met Office Unified Model, Quart. J. Roy. Meteor. Soc., 138, 1709–1720, 2012.

Würsch, M. and Craig, G. C.: A simple dynamical model of cumulus convection for data assimilation research, Meteorologische Zeitschrift, pp. 483–490, 2014.